GEOMETRY-AWARE HALLUCINATION DETECTION IN LARGE LANGUAGE MODELS

Anonymous authors
Paper under double-blind review

ABSTRACT

Large language models (LLMs) frequently generate factually incorrect or unsupported content, commonly referred to as hallucinations. Prior work has explored decoding strategies, retrieval augmentation, and supervised fine-tuning for hallucination detection, while recent studies show that in-context learning (ICL) can substantially influence factual reliability. However, existing ICL demonstration selection methods often rely on surface-level similarity heuristics and exhibit limited robustness across tasks and models.

We propose GA-ICL, a geometry-aware demonstration sampling framework for selecting in-context demonstrations that leverages latent representations extracted from frozen LLMs. By jointly modeling local manifold structure and class-aware prototype geometry, GA-ICL selects demonstrations based on their proximity to learned prototypes rather than lexical or embedding similarity alone.

Across factual verification (FEVER) and hallucination detection (HaluEval) benchmarks, GA-ICL outperforms standard ICL selection baselines in the majority of evaluated settings, with particularly strong gains on dialogue and summarization tasks. The method remains robust under temperature perturbations and model variation, indicating improved stability compared to heuristic retrieval strategies. While lexical retrieval can remain competitive in certain question-answering regimes at smaller model scales, our results demonstrate that geometry-aware prototype selection provides a reliable and training-light approach for hallucination detection without modifying LLM parameters. Extended evaluations on Phi-14B and Qwen3-32B confirm that GA-ICL scales effectively to larger models, outperforming all compared baselines including on QA tasks where smaller models show boundary-condition limitations, offering a principled direction for improved ICL demonstration selection.

1 INTRODUCTION

The rapid scaling of pre-trained language models (PLMs) has led to the emergence of new capabilities Wei et al. (2022), particularly through in-context learning (ICL), where models perform downstream tasks by conditioning on prompts that include a small number of representative examples. Owing to its effectiveness and flexibility, ICL has become a widely adopted and efficient paradigm for utilizing PLMs. This paradigm has been successfully applied to a variety of tasks, including reasoning and code generation Li et al. (2023a), Bodla & Yang (2025), mathematical reasoning Wu et al. (2025), and question answering Liu et al. (2023), among others, without requiring explicit supervised fine-tuning.

In this study, we investigate the use of in-context learning (ICL) as a mechanism for hallucination detection in large language models. Unlike many existing methods that target hallucination detection through architectural modifications or specialized training and inference Su et al. (2024) procedures, we examine whether leveraging ICL alone can provide comparable effectiveness for this task. Our experimental findings show that geometry-aware ICL yields gains over established baselines across a wide range of benchmarks and model configurations while attaining performance levels that are comparable to those achieved by supervised fine-tuning (Appendix C). Importantly, these results are obtained with lower computational costs, highlighting the suitability of our approach for deployment in resource-constrained environments.

Reviewers: please read the Reviewer Guidelines (iclr.cc/Conferences/2027/ReviewerGuidelines) and the AI Policy for Reviewers (iclr.cc/Conferences/2027/AIPolicyForReviewers). If you used AI to expand, edit, or polish your review, please provide the input text to the LLM. Better still, consider skipping the LLM and submitting your original text: we, and the authors, are much more interested in your unedited thoughts than in what an LLM has to say. AI-assisted or not, you are putting your name and reputation behind your review: LLM-generated falsehoods, hallucinations or misrepresentations are subject to disciplinary action, which may include desk-rejecting all papers you have authored.

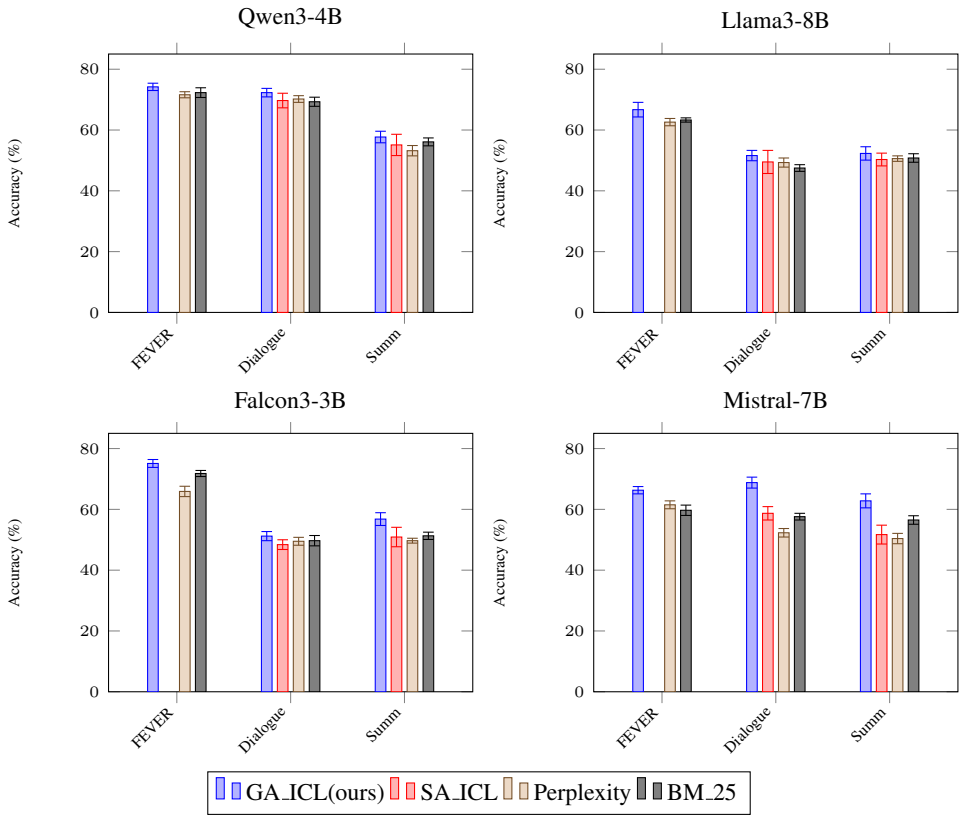

Figure 1: Accuracy comparison across models, broken down by dataset/task (FEVER, HaluEval Dialogue, HaluEval Summarization). Error bars denote standard deviation over 5 random seeds. SA_ICL has no reported score on FEVER.

Existing ICL demonstration selection strategies largely rely on distance-based retrieval in a fixed embedding space, using lexical similarity, or heuristic ranking criteria. While effective in some settings, such approaches implicitly assume that the raw embedding geometry is well aligned with factual consistency, which may not hold across tasks and models. We argue that semantic similarity alone is insufficient for hallucination detection because embedding proximity does not necessarily correspond to factual-consistency similarity. GA-ICL addresses this mismatch by learning a retrieval geometry explicitly optimized for hallucination-discriminative demonstration selection. Unlike prior ICL selection methods that operate purely via distance-based retrieval in a fixed embedding space, our approach learns the geometry used for selection itself by explicitly modeling local manifolds and prototype structure. This shifts ICL selection from heuristic similarity ranking to geometry-based prototype sampling, which, to our knowledge, has been underexplored for hallucination-aware ICL retrieval.

2 Method Overview

Given a dataset D, all textual fields are concatenated with a prompt template T_p (Appendix A), resulting in a transformed dataset containing a single consolidated text field F_t paired with its corresponding label l. The consolidated text field is passed through the corresponding LLM to obtain latent representations Z. The encoded latent representations Z are obtained by taking the final transformer layer's token hidden states and computing an attention mask weighted mean across all non padding tokens to produce a single fixed dimensional vector per input text. The extracted latent vector Z is used for all the comparison baselines, including ours, to sample the ICL demonstrations with respect to each LLM.

Algorithm: Training and Sampling Overview
Input: Dataset D_{F_T} with labels l, momentum coefficient μ
Output: Prototype representation θ_q and selected ICL demonstrations
Initialize projection network h_θ and prototype θ_q
for each batch $\mathcal{B} \subset D_{F_t}$ **do**
Obtain latent representations $Z \leftarrow \mathrm{LLM}(T)$
$Z' \leftarrow h_\theta(Z)$, Construct manifold structure for Z' (Section 2.1)
Compute loss: $\mathcal{L} = \mathcal{L}_{\text{manifold}} + \mathcal{L}_{\text{PA}}$, eq. 2 , 1
Update parameters of h_θ and θ_q via gradient descent
Update Momentum proxy He et al. (2020): $\theta_m \leftarrow \mu \cdot \theta_m + (1-\mu) \cdot \theta_q$
end for
Select ICL demonstrations by sampling representations Z' closest to θ_m

Table 1: Overview of the Proposed GA-ICL Algorithm.

As an initial step of our approach, we initialize a lightweight neural network h_θ (Table 2) that maps latent representations Z to transformed representations Z'. In addition, we initialize two proxy vectors θ_q, which serve as class representative prototypes within the proxy anchor loss, along with a momentum proxy vector θ_m that is updated according to the procedure outlined in Table 1. Upon completion of training, the learned momentum proxy θ_m is used to retrieve the nearest transformed representations Z', which are then selected as in context learning (ICL) demonstrations.

During training, for each mini batch $\mathcal{B} \subset D_{F_t}$, the latent representations Z are passed through h_θ to obtain transformed representations Z'. As described in Section 2.1, a manifold is then constructed for each batch based on Z'. The resulting manifold structure is used to compute the manifold point to point loss (Eq. 2), while the transformed representations Z' together with the proxy vectors θ_q are used to evaluate the proxy anchor loss (Eq. 1)

After computing both the manifold point to point loss and the proxy anchor loss, the overall training objective is formed as the sum of the two loss terms. The parameters of h_θ and the proxy vectors θ_q are then updated via gradient descent with respect to this combined loss, while the momentum proxy vector θ_m is updated following the procedure described in Table 1. Upon completion of training, the learned momentum proxy θ_m is used to retrieve the nearest transformed representations Z', which are selected as in context learning (ICL) demonstrations. The details of each parameter used and the training durations are clearly described in Appendix D.

We emphasize that our approach is not training free. Although the underlying language model remains fully frozen, our method requires training a lightweight retrieval module in the form of a projection network $h\theta$ and associated prototype representations. This training phase is performed once per dataset and model configuration and is substantially less expensive than fine tuning the language model itself. We therefore position GA-ICL as a training light rather than training free approach, operating in contrast to standard ICL methods that rely solely on heuristic or unsupervised retrieval without learned parameters.

Table 2: h_θ Model Architecture

Layer	**Layer Parameters**
Linear	(latent size Z, Prototype size Z')
InstanceNorm1d	Prototype size Z'
ReLU	-

2.1 Manifold Construction

Based on the Manifold hypothesis Cayton (2005), we can assume that the encoded latent representations can be locally approximated into smaller chunks of linear regions. This locally linear approximation follows the tradition of nonlinear dimensionality reduction methods such as Locally Linear Embedding Roweis & Saul (2000) and Laplacian Eigenmaps Belkin & Niyogi (2001),

which demonstrate that high-dimensional data concentrated near a lower-dimensional manifold can be faithfully represented through local linear patches. Our approach leverages this assumption Bhatnagar & Ahuja (2024), Holiday et al. (2019), Koronaki et al. (2023), Sonday et al. (2010) alongside prototype-based metric learning Snell et al. (2017) to identify representative prototypes that capture the characteristics of each class.

Anchor Initialization and Local Clustering To approximate the piecewise linear structure of the data, we aim to construct m-dimensional linear submanifolds around selected anchor points. Given a batch B containing N data points, we randomly select n anchor points. For each anchor point $h_\theta(Z_i)$, we identify its nearest $m-1$ neighbors using Euclidean distance and form an initial neighborhood set X_i.

Manifold Expansion and Validation After initializing the local clusters, the manifold construction process proceeds iteratively by attempting to add the m-th nearest neighbor to X_i. After each addition, we compute the best fit m-dimensional submanifold using PCA to assess whether the members of X_i can be reconstructed with quality above threshold $T\%$. If so, the m-th point is retained in X_i; otherwise it is excluded. This evaluation is repeated for subsequent neighbors $N(h_\theta(x_i))_j$ for $j \in \{m+1, \ldots, k\}$, gradually constructing a local linear approximation of the manifold.

Submanifold Basis Extraction The final set X_i is comprised of all points in the anchor point's neighborhood that lie well within an m-dimensional linear submanifold. A basis for this submanifold is computed by applying PCA on X_i and extracting the top m eigenvectors. PCA is well suited for this task because it can effectively construct the lower-dimensional manifolds for locally linear regions.

2.2 Training Objectives

Proxy Anchor Loss: We use a modified version of proxy anchor loss Kim et al. (2020) with Euclidean distance instead of cosine similarity:

$$\begin{aligned}\mathcal{L}_{\text{PA}} = \frac{1}{|\Theta_+|} \sum_{\theta_q \in \Theta_+} \log\Bigg(1 + \sum_{Z' \in \mathcal{Z}'^{+}_{\theta_q}} \exp\Big(-\alpha\big(\|h_\theta(Z) - \theta_q\|_2 - \epsilon\big)\Big)\Bigg) \\ + \frac{1}{|\Theta|} \sum_{\theta_q \in \Theta} \log\Bigg(1 + \sum_{Z' \in \mathcal{Z}'^{-}_{\theta_q}} \exp\Big(\alpha\big(\|h_\theta(Z) - \theta_q\|_2 - \epsilon\big)\Big)\Bigg)\end{aligned} \tag{1}$$

Let Θ represent the collection of all proxy vectors, where each proxy $\theta_q \in \Theta$ functions as a class-level representative in the embedding space. From this set, $\Theta_+ \subseteq \Theta$ denotes the subset of proxies that are associated with at least one positive sample within the current mini-batch B. For any selected proxy θ_q, the latent embeddings $\mathcal{Z}'$ contained in B (with $Z' \in \mathcal{Z}'$) are divided into two disjoint groups: the positive set $\mathcal{Z}'{\theta_q}^+$, consisting of embeddings from the same class as θ_q, and the negative set $\mathcal{Z}'{\theta_q}^- = \mathcal{Z}' \setminus \mathcal{Z}'^{+}_{\theta_q}$, which contains all remaining embeddings. The temperature parameter α regulates the concentration of the optimization process: larger values emphasize hard positive and negative pairs by sharpening gradients, whereas smaller values yield smoother updates by distributing influence more uniformly across pairs. The margin parameter ϵ introduces an explicit separation constraint, ensuring that embeddings from the same class are pulled closer to their corresponding proxies while embeddings from different classes are pushed beyond a minimum distance threshold.

Manifold Point-to-Point Loss: This loss helps in estimating the point to point similarities preserving the geometric structure:

$$\mathcal{L}_{\text{manifold}} = \sum_{i,j} \big(\delta \cdot (1 - s(Z'_i, Z'_j)) - \|h_\theta(Z_i) - h_\theta(Z_j)\|_2\big)^2 \tag{2}$$

where $s(Z'_i, Z'_j)$ is the manifold similarity computed as:

$$s(Z'_i, Z'_j) = \frac{s'(Z'_i, Z'_j) + s'(Z'_j, Z'_i)}{2}$$

with $s'(Z'_i, Z'_j) = \alpha(Z'_i, Z'_j) \cdot \beta(Z'_i, Z'_j)$, where:

$$\alpha(Z'_i, Z'_j) = \frac{1}{\left(1 + o(Z'_i, Z'_j)^2\right)^{N_\alpha}}$$
$$\beta(Z'_i, Z'_j) = \frac{1}{\left(1 + p(Z'_i, Z'_j)\right)^{N_\beta}}$$

In equation 2, h_θ denotes a lightweight neural transformation whose architecture is detailed in Table 2, and δ is a scaling constant that sets an upper bound on the separation between dissimilar samples. This objective aligns Euclidean distances in the transformed embedding space with manifold-induced dissimilarities $1 - s(Z'_i, Z'_j)$, thereby encouraging the learned metric to conform to the intrinsic geometry of the data manifold. The term $o(Z'_i, Z'_j)$ measures the orthogonal distance from point z_i to the manifold associated with Z'_j, while $p(Z'_i, Z'_j)$ captures the distance between Z'_j and the projection of z_i onto that manifold. The hyperparameters N_α and N_β regulate the rate at which similarity attenuates with increasing distance, with the constraint $N_\alpha > N_\beta$ ensuring that off-manifold points experience a steeper decay in similarity than points residing on the same manifold.

Distance Calculation. For each embedding pair (Z'_i, Z'_j), the distances $o(Z'_i, Z'_j)$ and $p(Z'_i, Z'_j)$ are computed using the local manifold basis P_j associated with point Z'_j. The projection of Z'_i onto the manifold spanned by P_j is defined as $\text{proj}_{P_j}(Z'_i) = Z'_j + \sum_k \langle Z'_i - Z'_j, v_k \rangle v_k$, where $\{v_k\}$ denotes the basis vectors of P_j. The orthogonal distance is then given by $o(Z'_i, Z'_j) = \|Z'_i - \text{proj}_{P_j}(Z'_i)\|_2$, while the projected distance along the manifold is defined as $p(Z'_i, Z'_j) = \|\text{proj}_{P_j}(Z'_i) - Z'_j\|_2$. This procedure is applied to all point pairs, enabling the loss to capture the local geometric structure of the data manifold.

3 EXPERIMENTS

We focus on hallucination detection, where the model predicts factual consistency labels, rather than modifying generation to reduce hallucinations. We conduct experiments across six large language models on hallucination detection (HaluEval) and factual verification (FEVER) tasks to evaluate our sampling approach. Demonstration selection, prompt construction, and decoding are all fixed across runs, and no stochastic sampling or retriever randomness is introduced. Our method (**GA-ICL**) attains higher accuracy relative to baseline methods in most of the scenarios. Additionally, lower perplexity scores compared to BM25 and self adaptive ICL sampling suggest reduced predictive uncertainty. To assess robustness to decoding stochasticity, we examine accuracy across different sampling temperatures. For the Qwen3-4B and Falcon3-3B models, our method shows limited sensitivity to temperature changes, in contrast to BM25 and self adaptive ICL based sampling methods, indicating more concentrated predictive distributions under typical inference settings. Our ablation study across all model parameters indicates that the prototype size Z' has the largest impact on performance (tuned on the validation split; Section 3.2). In particular, when the original latent dimension Z is substantially reduced to Z', we observe consistent changes in performance, suggesting the presence of manifold learning effects induced by the reduced representation capacity.

3.1 DATASET

We conduct experiments across four distinct tasks using six different large language models. The FEVER Thorne et al. (2018) dataset is a widely used benchmark for evaluating a model's ability to assess the factual correctness of a given sentence. It consists of two splits (train and test), where each instance contains a claim paired with a label indicating whether the statement is supported or refuted. The HaluEval Li et al. (2023b) dataset is comprised of 5,000 general user queries paired with ChatGPT-generated responses, along with 30,000 task specific examples spanning three

tasks: question answering, knowledge grounded dialogue conversation, and summarization. In the HaluEval question answering setting, the model is provided with a question, a supporting knowledge snippet, and a candidate answer, and is required to determine whether the answer is hallucinated. The dialogue and summarization subsets follow a similar format.

3.2 Evaluation details & Results

All sampling strategies, including our proposed method, were evaluated under a two shot in context learning (ICL) setting, where each method selected exactly two demonstrations per input across all models and tasks. This setup ensures that performance differences arise from the quality of the selected demonstrations rather than the quantity of contextual information provided to the model.

For the FEVER dataset, which includes predefined training and test splits, the training split was used exclusively for sampling ICL demonstrations, while evaluation was conducted on the held out test split. For HaluEval (summarization, QA, dialogue), which provides no official splits, we hold out a fixed 20% of each subset as the test set, the remaining 80% is used for training. All hyperparameter selection (prototype dimensionality Z', manifold and loss hyperparameters) is performed by further splitting this 80% into 65% train / 15% validation and selecting on validation accuracy; the 20% test set is identical across both configurations. For FEVER, we carve the 15% validation set out of the official training split and evaluate on the official test split. Test accuracy is reported exactly once per configuration, after all choices are fixed.

Table 3 summarizes the performance of all methods across six language models and four tasks. Across the majority of settings, our manifold based ICL sampling approach (GA-ICL) achieves higher accuracy than baseline retrieval and selection strategies, including BM25, perplexity based selection, clustering, and self-adaptive ICL (SA-ICL). GA-ICL improves hallucination detection accuracy across most models and tasks, with particularly strong gains in dialogue and summarization settings. To evaluate the scalability of our method on larger language models, we compared it against several baselines using Phi-14B and Qwen3-32B. As shown in Table 4, the results demonstrate that our method generalizes effectively to larger models.

GA-ICL improves performance across models and tasks in the majority of settings. On Mistral-7B, the method achieves large gains on dialogue and summarization hallucination detection, with absolute improvements of up to 10.1 accuracy points over standard retrieval baselines (Table 3). For Falcon3-3B, GA-ICL similarly yields clear improvements on the summarization task, where baseline selection strategies show limited effectiveness. In contrast, recent adaptive ICL selection methods generally report more modest gains, typically on the order of 1–2 percentage points, in comparable settings, highlighting the impact of effective demonstration selection for hallucination detection tasks. We note that in certain question-answering settings, lexical retrieval methods such as BM25 outperform GA-ICL, suggesting that surface level overlap can remain a strong signal when factual correctness is tightly coupled to explicit evidence matching.

To further examine the effect of the number of demonstrations, we conducted an ablation study varying the ICL shot count for the Qwen3-4B and Falcon3-3B models. As shown in Figures 4a and 4b, performance improves as the number of demonstrations increases up to approximately ten shots, after which gains begin to saturate. This trend is consistent across both dialogue and question answering tasks, indicating diminishing returns from additional demonstrations beyond this point. In addition to the experiments present in Section 3, we also present the effect of each loss component (Table 6) and the controlled random projection baseline on the encoded dimensions (Table 10).

Prototype dimensionality as a window into LLM hallucination geometry. Across both Qwen3-4B and Mistral-7B, reducing the prototype space to Z' from the full LLM hidden dimension is associated with improved hallucination detection accuracy across several settings (Figures 5b–5a). The magnitude of these gains is task-dependent: improvements are strongest on dialogue and summarization, where factual consistency requires reasoning over longer contexts, and weaker on QA, where explicit evidence snippets make lexical overlap a strong retrieval signal. While dimensionality reduction may also provide a regularization benefit, these results suggest that hallucination-relevant information can be effectively captured in a lower-dimensional learned representation. We therefore view the observed compression effect as evidence that compact retrieval geometries may help emphasize features that are useful for hallucination-aware demonstration selection.

Although our method includes an additional training stage to learn prototype representations, this overhead is offset by reduced inference-time retrieval cost. As shown in Appendix E, GA-ICL achieves lower inference time and memory consumption than the compared baselines in our experimental setting. This efficiency arises from its global sampling strategy, in which prototypes are selected once for the dataset and reused across test instances, avoiding the repeated per-query retrieval required by dynamically sampled baselines.

Finally, similar performance trends are observed across multiple model families and tasks, suggesting that the gains are not specific to a single architecture or evaluation setting. Collectively, these results support the effectiveness of manifold-based sampling for ICL demonstration selection in the hallucination detection settings considered here. All reported main results are obtained with the decoding temperature fixed at 0, making both demonstration selection and generation deterministic under the reported configuration. Robustness to decoding stochasticity is evaluated separately through temperature perturbation analysis, as reported in Section 3.3.

Model	Task	KNN	Clustering	BM25	Perplexity	SA-ICL	AdaICL	Top-k+Con-E	GA-ICL (Ours)
Qwen3-4B	HaluEval Dialogue	67.5 ± 1.2	50.1 ± 1.8	69.3 ± 1.5	70.2 ± 1.1	69.7 ± 2.4	68.6 ± 3.1	64.3 ± 1.9	$\mathbf{72.3 \pm 1.4}$
	HaluEval Summ.	53.9 ± 0.9	55.2 ± 2.1	56.1 ± 1.3	53.2 ± 1.7	55.1 ± 3.5	53.7 ± 2.2	53.5 ± 2.8	$\mathbf{57.7 \pm 1.9}$
	HaluEval QA	63.6 ± 1.6	50.5 ± 1.1	68.7 ± 0.8	$\mathbf{74.3 \pm 1.4}$	71.2 ± 1.8	67.6 ± 2.7	64.9 ± 3.9	71.2 ± 2.3
	FEVER	71.8 ± 1.1	69.8 ± 1.5	72.3 ± 1.6	71.6 ± 1.0	–	–	–	$\mathbf{74.2 \pm 1.2}$
Llama3-8B	HaluEval Dialogue	48.7 ± 1.4	50.2 ± 2.3	47.5 ± 1.1	49.3 ± 1.5	49.5 ± 3.8	$\mathbf{55.9 \pm 1.7}$	49.3 ± 2.5	51.6 ± 1.7
	HaluEval Summ.	51.2 ± 0.8	50.4 ± 1.7	50.8 ± 1.4	50.6 ± 0.9	50.3 ± 2.1	50.8 ± 3.3	50.1 ± 3.6	$\mathbf{52.3 \pm 2.2}$
	HaluEval QA	62.4 ± 1.7	51.7 ± 1.2	63.7 ± 1.2	61.8 ± 1.6	64.6 ± 2.9	62.5 ± 2.4	48.6 ± 1.8	$\mathbf{68.7 \pm 1.1}$
	FEVER	65.1 ± 1.3	63.3 ± 1.9	63.3 ± 0.7	62.6 ± 1.2	–	–	–	$\mathbf{66.7 \pm 2.4}$
Falcon-3-3B	HaluEval Dialogue	49.3 ± 1.5	50.3 ± 1.4	49.7 ± 1.7	49.5 ± 1.3	48.4 ± 1.6	50.4 ± 2.9	50.0 ± 3.1	$\mathbf{51.2 \pm 1.5}$
	HaluEval Summ.	50.8 ± 1.1	52.4 ± 2.0	51.3 ± 1.2	49.7 ± 0.8	50.9 ± 3.2	54.3 ± 2.1	52.3 ± 2.4	$\mathbf{56.8 \pm 2.1}$
	HaluEval QA	47.3 ± 0.9	50.3 ± 1.6	48.2 ± 1.5	49.7 ± 1.1	50.2 ± 2.5	50.5 ± 3.7	49.1 ± 1.7	$\mathbf{51.7 \pm 1.8}$
	FEVER	72.6 ± 1.4	72.3 ± 2.2	71.8 ± 1.0	65.9 ± 1.7	–	–	–	$\mathbf{75.1 \pm 1.3}$
GPT-Neo-2.7B	HaluEval Dialogue	–	50.3 ± 1.9	50.6 ± 1.3	48.5 ± 1.2	50.0 ± 3.4	49.8 ± 1.8	50.5 ± 2.2	$\mathbf{52.3 \pm 1.6}$
	HaluEval QA	–	50.4 ± 1.5	49.7 ± 0.9	46.2 ± 1.5	49.5 ± 2.7	49.3 ± 2.3	49.7 ± 3.5	$\mathbf{52.1 \pm 2.0}$
	FEVER	44.2 ± 1.2	50.2 ± 1.1	49.6 ± 1.6	49.2 ± 0.8	–	–	–	$\mathbf{51.3 \pm 1.1}$
Mistral-7B	HaluEval Dialogue	60.3 ± 1.6	50.4 ± 2.4	57.6 ± 1.1	52.3 ± 1.4	58.7 ± 2.2	57.7 ± 3.9	57.6 ± 2.6	$\mathbf{68.8 \pm 1.8}$
	HaluEval Summ.	40.2 ± 0.8	57.7 ± 1.3	56.5 ± 1.4	50.4 ± 1.7	51.7 ± 3.1	52.3 ± 1.6	55.6 ± 3.3	$\mathbf{62.8 \pm 2.3}$
	HaluEval QA	61.9 ± 1.3	51.3 ± 1.8	$\mathbf{66.3 \pm 1.0}$	52.0 ± 1.1	62.5 ± 1.9	60.1 ± 2.8	58.7 ± 2.1	62.3 ± 1.5
	FEVER	63.7 ± 1.5	64.3 ± 2.1	59.7 ± 1.7	61.5 ± 1.3	–	–	–	$\mathbf{66.3 \pm 1.2}$
Vicuna-7B	HaluEval Dialogue	47.8 ± 1.1	50.3 ± 1.7	49.5 ± 1.2	50.2 ± 0.9	50.4 ± 2.6	49.3 ± 3.2	49.7 ± 1.8	$\mathbf{51.6 \pm 2.1}$
	HaluEval Summ.	50.4 ± 1.4	51.3 ± 2.2	26.5 ± 1.5	51.3 ± 0.8	39.7 ± 3.7	53.3 ± 2.5	52.4 ± 2.9	$\mathbf{56.1 \pm 1.4}$
	HaluEval QA	49.1 ± 1.0	50.2 ± 1.3	49.8 ± 1.3	50.5 ± 1.6	50.3 ± 1.8	49.9 ± 2.1	50.2 ± 3.4	$\mathbf{51.8 \pm 1.9}$
	FEVER	66.3 ± 1.7	61.7 ± 1.6	67.8 ± 0.8	67.3 ± 1.4	–	–	–	$\mathbf{71.8 \pm 2.4}$

Table 3: Performance comparison (Accuracy)(mean $\pm$ std), for 5 random seeds, rounded off to nearest 1st floating point number

3.3 Effect of Temperature and Perplexity based evaluation

As an additional sanity check, we examined the effect of generation temperature on model behavior by varying the temperature from 0 to 1 in increments of 0.1. We compared the resulting output

Model	Task	Perplexity	SA-ICL	AdaICL	Top-k+Con-E	GA-ICL (Ours)
Phi-14B	HaluEval Dialogue	69.8 ± 0.5	72.3 ± 0.4	71.6 ± 0.4	65.1 ± 0.3	$\mathbf{75.6 \pm 0.4}$
	HaluEval Summ.	60.7 ± 0.4	59.2 ± 0.24	62.3 ± 0.2	62.3 ± 0.4	$\mathbf{65.6 \pm 0.3}$
	HaluEval QA	76.3 ± 0.2	78.5 ± 0.4	73.2 ± 0.2	76.8 ± 0.1	$\mathbf{81.3 \pm 0.3}$
Qwen3-32B	HaluEval Dialogue	80.3 ± 0.2	81.8 ± 0.3	81.1 ± 0.3	79.4 ± 0.2	$\mathbf{83.6 \pm 0.2}$
	HaluEval Summ.	63.6 ± 0.2	60.9 ± 0.2	60.2 ± 0.3	64.7 ± 0.1	$\mathbf{67.4 \pm 0.3}$
	HaluEval QA	66.3 ± 0.3	66.9 ± 0.2	65.3 ± 0.1	67.6 ± 0.2	$\mathbf{71.8 \pm 0.2}$

Table 4: Accuracy(mean $\pm$ std) comparison of GA-ICL on large scale models, performance averaged across 5 random seeds

variability of our method with that of **BM25** and **SA-ICL** on the HaluEval question answering and dialogue tasks Fig 6a, 6b, 7a, 7b. Across this range, our approach exhibited more stable behavior relative to the comparison methods. Specifically, as the temperature increased from $T = 0$ to $T = 1$, the variation in model outputs remained limited, suggesting that the sampling procedure is comparatively less sensitive to temperature changes.

This pattern is consistent with a more concentrated token probability distribution during generation. In addition to accuracy, we report average perplexity scores under fixed decoding conditions (temperature = 0) as a complementary diagnostic signal. Perplexity here is not interpreted as a calibrated measure of model uncertainty, but rather as an indicator of how well the selected in-context demonstrations align with the model's internal likelihood structure. Lower perplexity suggests that the resulting prompts induce outputs that are more consistent with the model's learned distribution, which empirically correlates with improved hallucination detection performance in our setting. Importantly, we treat perplexity as an observational metric and do not claim a causal relationship between perplexity reduction and factual correctness.

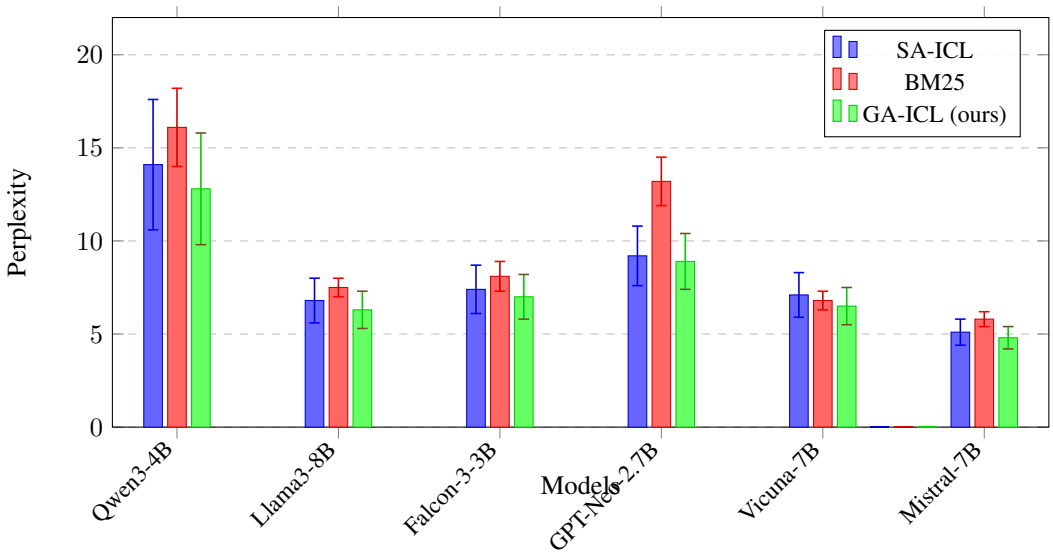

Figure 2: Perplexity comparison across models on HaluEval dialogue task. Lower perplexity indicates better performance.

4 Limitations and Future Works

GA-ICL's primary failure condition is structurally predictable from its design. On tasks where factual consistency is tightly coupled to surface-level lexical overlap between evidence and query most notably HaluEval QA, where each instance includes an explicit supporting knowledge snippet the geometry-aware geometric correction adds limited marginal value over lexical retrieval. In this

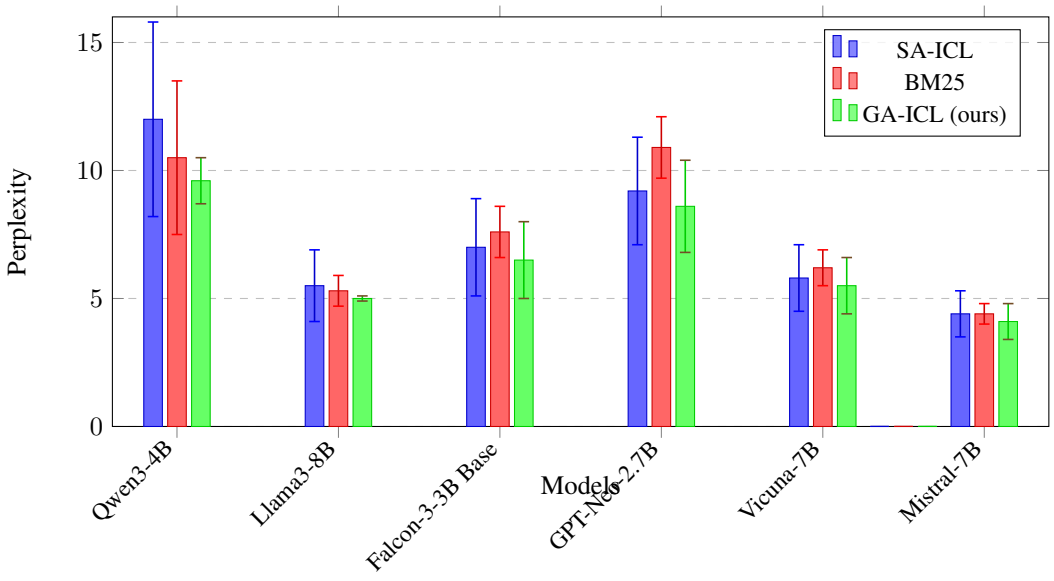

Figure 3: Perplexity comparison across models on HaluEval QA task. Lower perplexity indicates better performance.

structured evidence-matching regime, BM25's term-frequency matching already captures the task-relevant signal directly, and the lower-dimensional prototype space learned by GA-ICL does not meaningfully reorganize the geometry beyond what lexical overlap already provides. This boundary condition is constructive rather than limiting: it characterizes precisely the settings where GA-ICL is most valuable, namely open-ended dialogue and summarization tasks where factual consistency requires reasoning over longer context without explicit evidence anchoring. These are also the settings where deployed LLMs are most prone to hallucination in practice. Notably, this QA limitation diminishes at larger model scales on Phi-14B and Qwen3-32B, GA-ICL outperforms all baselines including on QA, suggesting that richer latent geometries in larger models provide more compressible hallucination-relevant structure even in evidence-grounded settings.

4.1 Future works

GA-ICL introduces a one-time training cost of 3–4 hours and 640MB GPU memory per dataset-model pair, which, while substantially lower than fine-tuning, is an overhead absent from purely heuristic methods. Additionally, the current framework does not support adaptive prototype updates at inference time, which may limit robustness in dynamic or streaming deployment scenarios. A promising direction for future work is the development of dynamic query-aware prototype selection strategies. In the current framework, prototypes are sampled globally and reused across all test instances, which significantly improves inference efficiency. A natural extension of the dimensionality finding reported here is a systematic study of which attention heads or transformer layers concentrate hallucination-discriminative geometry, which could inform more targeted compression strategies. Another important direction is extending GA-ICL to multimodal hallucination detection settings. While our current work focuses exclusively on textual hallucinations, modern large multimodal models frequently generate hallucinated content in image captioning, visual question answering, and video understanding tasks. Future research could explore whether geometry-aware prototype sampling can effectively model cross-modal latent geometries by jointly leveraging textual and visual representations. This extension may provide a scalable and training-light framework for improving factual reliability in multimodal generative systems.

AI USE STATEMENT

We have used AI tools for writing assistance. We did not use it during any of the ideation or experimentation phase.

REPRODUCIBILITY STATEMENT

The complete details of the implementation and all the hyperparameter settings are specified in the section D. We also submit the codes used for our experiments in the supplementary materials.

REFERENCES

Mikhail Belkin and Partha Niyogi. Laplacian eigenmaps and spectral techniques for embedding and clustering. In T. Dietterich, S. Becker, and Z. Ghahramani (eds.), *Advances in Neural Information Processing Systems*, volume 14. MIT Press, 2001. URL https://proceedings.neurips.cc/paper_files/paper/2001/file/f106b7f99d2cb30c3db1c3cc0fde9ccb-Paper.pdf.

Shubhang Bhatnagar and Narendra Ahuja. Piecewise-linear manifolds for deep metric learning, 2024. URL https://arxiv.org/abs/2403.14977.

Krishna Vamshi Bodla and Haizhao Yang. Protocode: Prototype-driven interpretability for code generation in llms, 2025. URL https://arxiv.org/abs/2509.25247.

Tom B. Brown, Benjamin Mann, Nick Ryder, Melanie Subbiah, Jared Kaplan, Prafulla Dhariwal, Arvind Neelakantan, Pranav Shyam, Girish Sastry, Amanda Askell, Sandhini Agarwal, Ariel Herbert-Voss, Gretchen Krueger, Tom Henighan, Rewon Child, Aditya Ramesh, Daniel M. Ziegler, Jeffrey Wu, Clemens Winter, Christopher Hesse, Mark Chen, Eric Sigler, Mateusz Litwin, Scott Gray, Benjamin Chess, Jack Clark, Christopher Berner, Sam McCandlish, Alec Radford, Ilya Sutskever, and Dario Amodei. Language models are few-shot learners, 2020. URL https://arxiv.org/abs/2005.14165.

Lawrence Cayton. Algorithms for manifold learning. 07 2005.

Anthony Chen, Panupong Pasupat, Sameer Singh, Hongrae Lee, and Kelvin Guu. Purr: Efficiently editing language model hallucinations by denoising language model corruptions, 2023. URL https://arxiv.org/abs/2305.14908.

I-Chun Chern, Steffi Chern, Shiqi Chen, Weizhe Yuan, Kehua Feng, Chunting Zhou, Junxian He, Graham Neubig, and Pengfei Liu. Factool: Factuality detection in generative ai – a tool augmented framework for multi-task and multi-domain scenarios, 2023. URL https://arxiv.org/abs/2307.13528.

Yung-Sung Chuang, Yujia Xie, Hongyin Luo, Yoon Kim, James Glass, and Pengcheng He. Dola: Decoding by contrasting layers improves factuality in large language models, 2024. URL https://arxiv.org/abs/2309.03883.

Qingxiu Dong, Lei Li, Damai Dai, Ce Zheng, Jingyuan Ma, Rui Li, Heming Xia, Jingjing Xu, Zhiyong Wu, Tianyu Liu, Baobao Chang, Xu Sun, Lei Li, and Zhifang Sui. A survey on in-context learning, 2024. URL https://arxiv.org/abs/2301.00234.

Mohamed Elaraby, Mengyin Lu, Jacob Dunn, Xueying Zhang, Yu Wang, Shizhu Liu, Pingchuan Tian, Yuping Wang, and Yuxuan Wang. Halo: Estimation and reduction of hallucinations in open-source weak large language models, 2023. URL https://arxiv.org/abs/2308.11764.

Hila Gonen, Srini Iyer, Terra Blevins, Noah Smith, and Luke Zettlemoyer. Demystifying prompts in language models via perplexity estimation. In Houda Bouamor, Juan Pino, and Kalika Bali (eds.), *Findings of the Association for Computational Linguistics: EMNLP 2023*, pp. 10136–10148, Singapore, December 2023. Association for Computational Linguistics. doi: 10.18653/v1/2023.findings-emnlp.679. URL https://aclanthology.org/2023.findings-emnlp.679/.

Kaiming He, Haoqi Fan, Yuxin Wu, Saining Xie, and Ross Girshick. Momentum contrast for unsupervised visual representation learning, 2020. URL https://arxiv.org/abs/1911.05722.

Alexander Holiday, Mahdi Kooshkbaghi, Juan M. Bello-Rivas, C. William Gear, Antonios Zagaris, and Ioannis G. Kevrekidis. Manifold learning for parameter reduction. *Journal of Computational Physics*, 392:419–431, 2019. ISSN 0021-9991. doi: https://doi.org/10.1016/j.jcp.2019.04.015. URL https://www.sciencedirect.com/science/article/pii/S0021999119302487.

Adam Tauman Kalai, Ofir Nachum, Santosh S. Vempala, and Edwin Zhang. Why language models hallucinate, 2025. URL https://arxiv.org/abs/2509.04664.

Sungyeon Kim, Dongwon Kim, Minsu Cho, and Suha Kwak. Proxy anchor loss for deep metric learning, 2020. URL https://arxiv.org/abs/2003.13911.

Eleni D. Koronaki, Nikolaos Evangelou, Cristina P. Martin-Linares, Edriss S. Titi, and Ioannis G. Kevrekidis. Nonlinear dimensionality reduction then and now: Aims for dissipative pdes in the ml era, 2023. URL https://arxiv.org/abs/2310.15816.

Jia Li, Ge Li, Chongyang Tao, Jia Li, Huangzhao Zhang, Fang Liu, and Zhi Jin. Large language model-aware in-context learning for code generation, 2023a. URL https://arxiv.org/abs/2310.09748.

Junyi Li, Xiaoxue Cheng, Xin Zhao, Jian-Yun Nie, and Ji-Rong Wen. HaluEval: A large-scale hallucination evaluation benchmark for large language models. In Houda Bouamor, Juan Pino, and Kalika Bali (eds.), *Proceedings of the 2023 Conference on Empirical Methods in Natural Language Processing*, pp. 6449–6464, Singapore, December 2023b. Association for Computational Linguistics. doi: 10.18653/v1/2023.emnlp-main.397. URL https://aclanthology.org/2023.emnlp-main.397/.

Xiaonan Li, Kai Lv, Hang Yan, Tianyang Lin, Wei Zhu, Yuan Ni, Guotong Xie, Xiaoling Wang, and Xipeng Qiu. Unified demonstration retriever for in-context learning. In Anna Rogers, Jordan Boyd-Graber, and Naoaki Okazaki (eds.), *Proceedings of the 61st Annual Meeting of the Association for Computational Linguistics (Volume 1: Long Papers)*, pp. 4644–4668, Toronto, Canada, July 2023c. Association for Computational Linguistics. doi: 10.18653/v1/2023.acl-long.256. URL https://aclanthology.org/2023.acl-long.256/.

Jiachang Liu, Dinghan Shen, Yizhe Zhang, Bill Dolan, Lawrence Carin, and Weizhu Chen. What makes good in-context examples for GPT-3? In Eneko Agirre, Marianna Apidianaki, and Ivan Vulić (eds.), *Proceedings of Deep Learning Inside Out (DeeLIO 2022): The 3rd Workshop on Knowledge Extraction and Integration for Deep Learning Architectures*, pp. 100–114, Dublin, Ireland and Online, May 2022. Association for Computational Linguistics. doi: 10.18653/v1/2022.deelio-1.10. URL https://aclanthology.org/2022.deelio-1.10/.

Weihao Liu, Fangyu Lei, Tongxu Luo, Jiahe Lei, Shizhu He, Jun Zhao, and Kang Liu. Mmhqa-icl: Multimodal in-context learning for hybrid question answering over text, tables and images, 2023. URL https://arxiv.org/abs/2309.04790.

Junyu Luo, Cao Xiao, and Fenglong Ma. Zero-resource hallucination prevention for large language models, 2023. URL https://arxiv.org/abs/2309.02654.

Potsawee Manakul, Adian Liusie, and Mark J. F. Gales. Selfcheckgpt: Zero-resource black-box hallucination detection for generative large language models, 2023. URL https://arxiv.org/abs/2303.08896.

Costas Mavromatis, Balasubramaniam Srinivasan, Zhengyuan Shen, Jiani Zhang, Huzefa Rangwala, Christos Faloutsos, and George Karypis. Which examples to annotate for in-context learning? towards effective and efficient selection, 2023. URL https://arxiv.org/abs/2310.20046.

Sewon Min, Kalpesh Krishna, Xinxi Lyu, Mike Lewis, Wen tau Yih, Pang Wei Koh, Mohit Iyyer, Luke Zettlemoyer, and Hannaneh Hajishirzi. Factscore: Fine-grained atomic evaluation of factual precision in long form text generation, 2023. URL https://arxiv.org/abs/2305.14251.

Dor Muhlgay, Ori Ram, Inbal Magar, Yoav Levine, Nir Ratner, Yonatan Belinkov, Omri Abend, Kevin Leyton-Brown, Amnon Shashua, and Yoav Shoham. Generating benchmarks for factuality evaluation of language models, 2024. URL https://arxiv.org/abs/2307.06908.

Baolin Peng, Michel Galley, Pengcheng He, Hao Cheng, Yujia Xie, Yu Hu, Qiuyuan Huang, Lars Liden, Zhou Yu, Weizhu Chen, and Jianfeng Gao. Check your facts and try again: Improving large language models with external knowledge and automated feedback, 2023. URL https://arxiv.org/abs/2302.12813.

Keqin Peng, Liang Ding, Yancheng Yuan, Xuebo Liu, Min Zhang, Yuanxin Ouyang, and Dacheng Tao. Revisiting demonstration selection strategies in in-context learning, 2024. URL https://arxiv.org/abs/2401.12087.

Chengwei Qin, Aston Zhang, Chen Chen, Anirudh Dagar, and Wenming Ye. In-context learning with iterative demonstration selection, 2024. URL https://arxiv.org/abs/2310.09881.

Vipula Rawte, S. M Towhidul Islam Tonmoy, Krishnav Rajbangshi, Shravani Nag, Aman Chadha, Amit P. Sheth, and Amitava Das. Factoid: Factual entailment for hallucination detection, 2024. URL https://arxiv.org/abs/2403.19113.

Sam T. Roweis and Lawrence K. Saul. Nonlinear dimensionality reduction by locally linear embedding. *Science*, 290(5500):2323–2326, 2000. doi: 10.1126/science.290.5500.2323. URL https://www.science.org/doi/abs/10.1126/science.290.5500.2323.

Ohad Rubin, Jonathan Herzig, and Jonathan Berant. Learning to retrieve prompts for in-context learning. In Marine Carpuat, Marie-Catherine de Marneffe, and Ivan Vladimir Meza Ruiz (eds.), *Proceedings of the 2022 Conference of the North American Chapter of the Association for Computational Linguistics: Human Language Technologies*, pp. 2655–2671, Seattle, United States, July 2022. Association for Computational Linguistics. doi: 10.18653/v1/2022.naacl-main.191. URL https://aclanthology.org/2022.naacl-main.191/.

Pranab Sahoo, Prabhash Meharia, Akash Ghosh, Sriparna Saha, Vinija Jain, and Aman Chadha. A comprehensive survey of hallucination in large language, image, video and audio foundation models. In Yaser Al-Onaizan, Mohit Bansal, and Yun-Nung Chen (eds.), *Findings of the Association for Computational Linguistics: EMNLP 2024*, pp. 11709–11724, Miami, Florida, USA, November 2024. Association for Computational Linguistics. doi: 10.18653/v1/2024.findings-emnlp.685. URL https://aclanthology.org/2024.findings-emnlp.685/.

Jake Snell, Kevin Swersky, and Richard S. Zemel. Prototypical networks for few-shot learning, 2017. URL https://arxiv.org/abs/1703.05175.

Benjamin E. Sonday, Amit Singer, C. William Gear, and Ioannis G. Kevrekidis. Manifold learning techniques and model reduction applied to dissipative pdes, 2010. URL https://arxiv.org/abs/1011.5197.

Taylor Sorensen, Joshua Robinson, Christopher Rytting, Alexander Shaw, Kyle Rogers, Alexia Delorey, Mahmoud Khalil, Nancy Fulda, and David Wingate. An information-theoretic approach to prompt engineering without ground truth labels. In Smaranda Muresan, Preslav Nakov, and Aline Villavicencio (eds.), *Proceedings of the 60th Annual Meeting of the Association for Computational Linguistics (Volume 1: Long Papers)*, pp. 819–862, Dublin, Ireland, May 2022. Association for Computational Linguistics. doi: 10.18653/v1/2022.acl-long.60. URL https://aclanthology.org/2022.acl-long.60/.

Weihang Su, Changyue Wang, Qingyao Ai, Yiran Hu, Zhijing Wu, Yujia Zhou, and Yiqun Liu. Unsupervised real-time hallucination detection based on the internal states of large language models. In Lun-Wei Ku, Andre Martins, and Vivek Srikumar (eds.), *Findings of the Association for Computational Linguistics: ACL 2024*, pp. 14379–14391, Bangkok, Thailand, August

2024. Association for Computational Linguistics. doi: 10.18653/v1/2024.findings-acl.854. URL https://aclanthology.org/2024.findings-acl.854/.

Eshaan Tanwar, Subhabrata Dutta, Manish Borthakur, and Tanmoy Chakraborty. Multilingual LLMs are better cross-lingual in-context learners with alignment. In Anna Rogers, Jordan Boyd-Graber, and Naoaki Okazaki (eds.), *Proceedings of the 61st Annual Meeting of the Association for Computational Linguistics (Volume 1: Long Papers)*, pp. 6292–6307, Toronto, Canada, July 2023. Association for Computational Linguistics. doi: 10.18653/v1/2023.acl-long.346. URL https://aclanthology.org/2023.acl-long.346/.

James Thorne, Andreas Vlachos, Christos Christodoulopoulos, and Arpit Mittal. FEVER: a large-scale dataset for fact extraction and VERification. In Marilyn Walker, Heng Ji, and Amanda Stent (eds.), *Proceedings of the 2018 Conference of the North American Chapter of the Association for Computational Linguistics: Human Language Technologies, Volume 1 (Long Papers)*, pp. 809–819, New Orleans, Louisiana, June 2018. Association for Computational Linguistics. doi: 10.18653/v1/N18-1074. URL https://aclanthology.org/N18-1074/.

Neeraj Varshney, Wenlin Yao, Hongming Zhang, Jianshu Chen, and Dong Yu. A stitch in time saves nine: Detecting and mitigating hallucinations of llms by validating low-confidence generation, 2023. URL https://arxiv.org/abs/2307.03987.

Xinyi Wang, Wanrong Zhu, Michael Saxon, Mark Steyvers, and William Yang Wang. Large language models are latent variable models: Explaining and finding good demonstrations for incontext learning, 2024. URL https://arxiv.org/abs/2301.11916.

Jason Wei, Yi Tay, Rishi Bommasani, Colin Raffel, Barret Zoph, Sebastian Borgeaud, Dani Yogatama, Maarten Bosma, Denny Zhou, Donald Metzler, Ed H. Chi, Tatsunori Hashimoto, Oriol Vinyals, Percy Liang, Jeff Dean, and William Fedus. Emergent abilities of large language models, 2022. URL https://arxiv.org/abs/2206.07682.

Patrick H. Winston. Learning and reasoning by analogy. *Commun. ACM*, 23(12):689–703, December 1980. ISSN 0001-0782. doi: 10.1145/359038.359042. URL https://doi.org/10.1145/359038.359042.

Jinyang Wu, Mingkuan Feng, Shuai Zhang, Feihu Che, Zengqi Wen, Chonghua Liao, and Jianhua Tao. Beyond examples: High-level automated reasoning paradigm in in-context learning via mcts, 2025. URL https://arxiv.org/abs/2411.18478.

Zhiyong Wu, Yaoxiang Wang, Jiacheng Ye, and Lingpeng Kong. Self-adaptive in-context learning: An information compression perspective for in-context example selection and ordering. In Anna Rogers, Jordan Boyd-Graber, and Naoaki Okazaki (eds.), *Proceedings of the 61st Annual Meeting of the Association for Computational Linguistics (Volume 1: Long Papers)*, pp. 1423–1436, Toronto, Canada, July 2023. Association for Computational Linguistics. doi: 10.18653/v1/2023.acl-long.79. URL https://aclanthology.org/2023.acl-long.79/.

Jiacheng Ye, Zhiyong Wu, Jiangtao Feng, Tao Yu, and Lingpeng Kong. Compositional exemplars for in-context learning. In Andreas Krause, Emma Brunskill, Kyunghyun Cho, Barbara Engelhardt, Sivan Sabato, and Jonathan Scarlett (eds.), *Proceedings of the 40th International Conference on Machine Learning*, volume 202 of *Proceedings of Machine Learning Research*, pp. 39818–39833. PMLR, 23–29 Jul 2023. URL https://proceedings.mlr.press/v202/ye23c.html.

Shuo Zhang, Liangming Pan, Junzhou Zhao, and William Yang Wang. The knowledge alignment problem: Bridging human and external knowledge for large language models, 2024. URL https://arxiv.org/abs/2305.13669.

Yiming Zhang, Shi Feng, and Chenhao Tan. Active example selection for in-context learning. In Yoav Goldberg, Zornitsa Kozareva, and Yue Zhang (eds.), *Proceedings of the 2022 Conference on Empirical Methods in Natural Language Processing*, pp. 9134–9148, Abu Dhabi, United Arab Emirates, December 2022. Association for Computational Linguistics. doi: 10.18653/v1/2022.emnlp-main.622. URL https://aclanthology.org/2022.emnlp-main.622/.

A PROMPT TEMPLATES

The following is the prompt template that we used in our experiments to combine the sampled ICL demonstrations with the test query, all the models and baseline methods, including ours, follow the same prompt template.

Listing 1: ICL prompt construction for Halueval QA task

```
def build_icl_prompt(knowledges, questions, answers, few_shots=None):
    prompt = (
        "You are an unbiased document-grounded fact checker. "
        "You are provided a Knowledge, a question based on the knowledge and a answe
        "Based on the provided knowledge for the question identify if the correspondi
        "Hallucination response: 'yes' = hallucinated, 'no' = not hallucinated.\n\n"
    )

    if few_shots:
        for know, ques, ans, label in few_shots:
            prompt += (
                f"Knowledge: {know}\n"
                f"Question: {ques}\n"
                f"Answer: {ans}\n"
                f"Hallucination response: [BEGIN]{label}[DONE]\n\n"
            )

    prompt += (
        f"Knowledge: {knowledges}\n"
        f"question: {questions}\n"
        f"Answer: {answers}\n"
        "Hallucination response: [BEGIN]"
    )

    return prompt
```

Listing 2: ICL prompt construction for HaluEval Dialogue task

```
def build_icl_prompt(knowledges, diag_hists, responses, few_shots=None):
    prompt = (
        "You are an unbiased document-grounded fact checker. "
        "You are provided a Knowledge, a dialogue history based on the knowledge and
        "based on the Knowledge and the dialogue history. "
        "Based on the provided knowledge and dialogue history identify if the corresp
        "response is hallucinated or not.\n"
        "Hallucination response: 'yes' = hallucinated, 'no' = not hallucinated.\n\n"
    )

    if few_shots:
        for know, diag_hist, res, label in few_shots:
            prompt += (
                f"Knowledge: {know}\n"
                f"Dialogue history: {diag_hist}\n"
                f"Response: {res}\n"
                f"Hallucination response: [BEGIN]{label}[DONE]\n\n"
            )

    prompt += (
        f"Knowledge: {knowledges}\n"
        f"Dialogue history: {diag_hists}\n"
        f"Response: {responses}\n"
        "Hallucination response: [BEGIN]"
```

```
    )

    return prompt
```

Listing 3: ICL prompt construction for HaluEval Summarization task

```
def build_icl_prompt(documents, summaries, few_shots=None):
    prompt = (
        "You are an unbiased document-grounded fact checker. "
        "Identify if the corresponding summary for the given document "
        "is hallucinated or not.\n"
        "Hallucination response: 'yes' = hallucinated, "
        "'no' = not hallucinated.\n\n"
    )

    if few_shots:
        for doc, summary, label in few_shots:
            prompt += (
                f"Document: {doc}\n"
                f"Summary: {summary}\n"
                f"Hallucination response: [BEGIN]{label}[DONE]\n\n"
            )

    prompt += (
        f"Document: {documents}\n"
        f"Summary: {summaries}\n"
        "Hallucination response: [BEGIN]"
    )

    return prompt
```

Listing 4: ICL prompt construction for FEVER dataset

```
def build_icl_prompt(test_problem, few_shots=None):
    prompt = ""
    if few_shots:
        for prob, sol in few_shots:
            prompt += (
                "You are an unbiased fact checker. "
                "Classify the following claim as supported if it is valid "
                "or refuted if it is invalid:\n"
                f"Claim: {prob}\n"
                "[BEGIN]\n"
                f"{sol}\n"
                "[DONE]\n\n"
            )

    prompt += (
        "You are an unbiased fact checker. "
        "Classify the following claim as supported if it is valid "
        "or refuted if it is invalid:\n"
        f"Claim: {test_problem}\n"
        "[BEGIN]\n"
    )

    return prompt
```

B Related Works

B.1 In-Context learning

In-context learning (ICL) Brown et al. (2020) describes a paradigm in which language models solve tasks by relying on a limited set of example demonstrations provided at inference time, without modifying their internal parameters. Since these demonstrations are expressed directly in natural language, ICL enables an intuitive and interpretable mode of interaction with large language models (LLMs). This paradigm also aligns with key aspects of human cognition, particularly analogical reasoning, where prior examples inform decision-making in new situations Winston (1980). Unlike conventional supervised learning approaches, ICL does not require additional training or fine-tuning, allowing models to flexibly generalize to novel tasks without incurring extra computational cost.

Building on these observations, numerous unsupervised methods have been proposed to identify informative demonstrations for in-context learning, as reviewed by Dong et al. (2024). One common line of work focuses on retrieving demonstrations that are closely related to the test input under predefined notions of similarity (Liu et al. (2022), Tanwar et al. (2023), Qin et al. (2024)). These approaches typically measure proximity using embedding-based distances, such as cosine similarity or Euclidean (L2) distance. Beyond similarity driven retrieval, prior studies have also explored alternative selection signals, including mutual information Sorensen et al. (2022) and perplexity Gonen et al. (2023), which enable effective prompt construction without requiring labeled supervision or access to a model's internal parameters.

Although widely used in practice, generic retrieval based strategies often depend on heuristic design choices and can produce suboptimal in context examples due to the absence of explicit task level supervision. Importantly, these approaches typically assume that semantic similarity in the original embedding space is aligned with factual consistency, an assumption that may not hold for hallucination detection. To overcome these limitations, prior work has explored supervised retriever based methods for demonstration selection (Rubin et al. (2022), Ye et al. (2023), Wang et al. (2024), Zhang et al. (2022)). One representative approach is EPR proposed by Rubin et al. (2022), which employs a two stage training procedure to learn dense retrievers tailored for demonstration retrieval. Building on this idea, Li et al. (2023c) introduced a unified retrieval model capable of handling demonstration selection across diverse tasks. More recently, Mavromatis et al. (2023) proposed AdaICL, a model aware framework that leverages LLM generated pseudo labels and uncertainty estimates over unlabeled data to adaptively identify informative in context demonstrations.

B.2 Hallucination detection

Identifying hallucinations in large language models is essential for maintaining the trustworthiness and reliability of their generated outputs, particularly in settings where factual accuracy is critical. SelfCheckGPT Manakul et al. (2023) introduces a zero-resource, black-box framework for hallucination detection that operates without access to external knowledge bases. The method is grounded in the observation that when a model has sufficient familiarity with a topic, it tends to produce internally consistent factual statements across multiple generations, whereas responses generated for less familiar content are more likely to exhibit inconsistencies or unsupported claims. The FACTOR Muhlgay et al. (2024) framework evaluates factuality by transforming a factual corpus into controlled multiple-choice benchmarks, generating plausible false alternatives and measuring whether a model assigns higher likelihood to true facts, which enables scalable assessment of factual accuracy without requiring external validation at generation time.

FActScore Min et al. (2023) introduces a fine-grained evaluation metric by decomposing long-form text into atomic facts and computing the percentage of these facts supported by a trusted knowledge source, with an automated estimator that approximates human judgments efficiently. FACTOID Rawte et al. (2024) reframes hallucination detection as a factual entailment problem, jointly identifying whether text is factually supported and localizing specific spans that contain errors, thereby improving upon traditional entailment models for fine-grained factual verification. Finally, FacTool Chern et al. (2023) builds a task-agnostic, tool-augmented framework that extracts claims from generated outputs and verifies them using appropriate external tools such as search engines or execution environments, grounding factuality judgments in collected evidence rather than model-internal signals alone.

Method	Memory (GB)	Time (hrs)	Acc
LoRA-SFT, 4-bit	24	2.6	0.71
LoRA-SFT, 8-bit	40	3.6	0.74
LoRA-SFT, 16-bit	72	4.1	0.73
GA-ICL (ours)	0.64	3.4	0.71

Table 5: Comparison of computational cost and performance between supervised fine-tuning (SFT) and GA-ICL for Vicuna-7B model. GA-ICL achieves comparable performance with orders-of-magnitude lower GPU memory usage.

In Kalai et al. (2025), the authors argue that a primary factor contributing to hallucinated yet seemingly plausible outputs in large language models is the mismatch between training and inference objectives. Specifically, these objectives tend to incentivize confident guessing rather than explicit acknowledgment of uncertainty, which in turn complicates the identification of the underlying causes of hallucinations. To address the generation of hallucinated content, a wide range of mitigation strategies have been proposedSahoo et al. (2024). These approaches include, but are not limited to, data augmentation and manipulation techniques Peng et al. (2023), Chuang et al. (2024), alignment and fine-tuning strategies Chen et al. (2023), Zhang et al. (2024), as well as prompt engineering based methods Varshney et al. (2023), Luo et al. (2023), Elaraby et al. (2023).

C Performance Considerations

A popular approach to mitigating hallucinations in LLMs is fine-tuning, which modifies the underlying model weights to align with factual distributions. While effective, fine-tuning requires significant GPU memory and multiple training iterations. In contrast, our proposed manifold based sampling framework operates as a lightweight retrieval mechanism that achieves comparable performance gains using a fraction of the resources. By training only a thin projection head h_θ (see Table 2) and keeping the base model frozen, our method reduces the training memory footprint by several orders of magnitude, making GA-ICL suitable for domain-specific hallucination where fine-tuning is impractical.

We evaluate the performance of GA-ICL against a fine-tuned baseline. All experiments are conducted on Vicuna-7B using A6000 RTX GPUs with 48 GB of memory. Fine-tuning the 16-bit model requires two GPUs, while all other fine-tuning configurations are run on a single GPU. For each model, we attached LoRA adapters to the last 3 to 5 layers, including the highest performing configuration in Table 5. A summary of experiment configurations and computational results is provided in Table 5.

C.1 Comparison methods

We compare our approach against five baseline sampling methods. **KNN** selects the most similar example(s) from the dataset for each query based on cosine similarity. **Clustering** chooses examples that are closest to the class centroid within each group. We note that clustering-based selection often performs near chance level in hallucination detection settings, reflecting the limited alignment between global semantic clusters and factual consistency labels. The **Perplexity** Gonen et al. (2023) based method follows prior work on perplexity driven selection, where all input fields except the label are concatenated into a text prompt and passed through the corresponding LLM to compute perplexity scores. Prompts with the lowest perplexity values are then selected as in context learning (ICL) demonstrations. **BM25** is a lexical similarity based retrieval method that ranks candidate examples using term frequency inverse document frequency (TF–IDF) statistics and selects the top scoring examples as demonstrations. **SA-ICL** (Self-Adaptive ICL) Wu et al. (2023) is based on prior self-adaptive ICL work, where the top-k relevant demonstrations for each test query are first retrieved using similarity measures and subsequently reordered to obtain an arrangement that minimizes the code length of the label Y, following the Minimum Description Length (MDL) principle. **AdaICL** Mavromatis et al. (2023) identifies "hard" examples ones the LLM is most uncertain about (low max confidence over labels) then uses a greedy Maximum Coverage algorithm over their SBERT-based neighborhood graph to select a diverse, representative annotation budget. At infer-

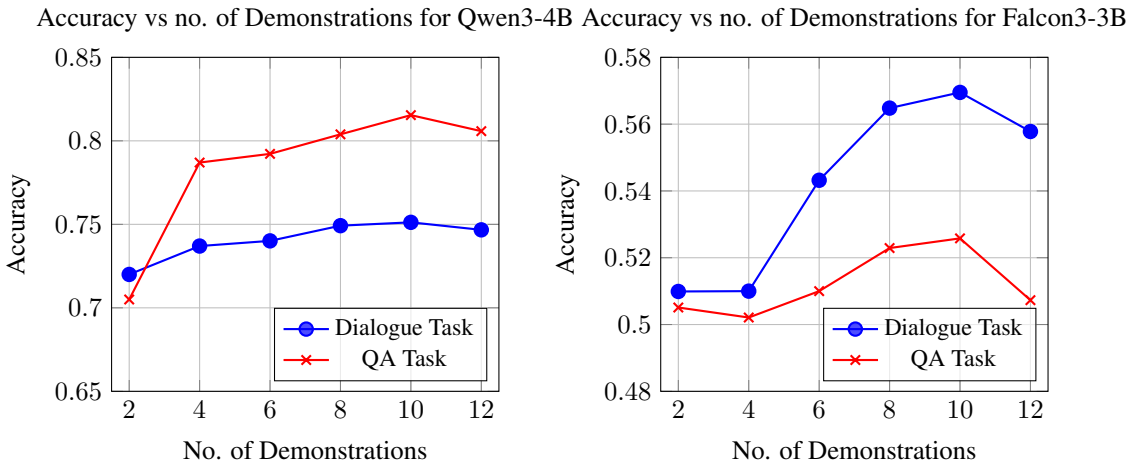

(a) Qwen3-4B (b) Falcon3-3B

Figure 4: Performance of GA-ICL under varying numbers of in-context demonstrations

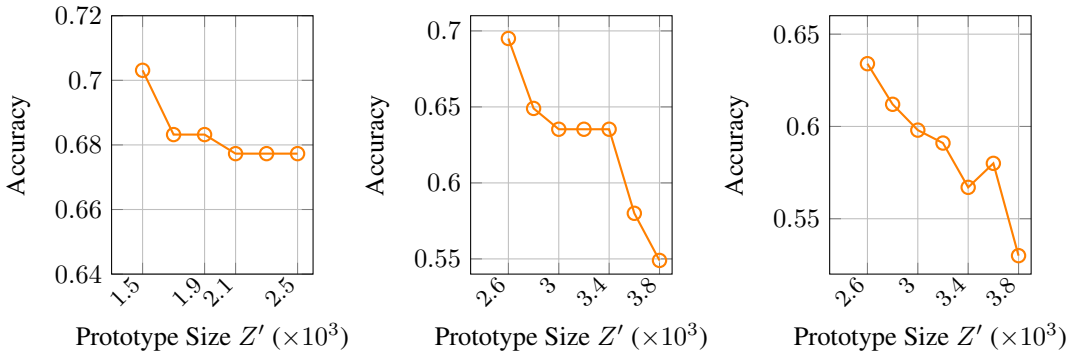

(a) Qwen3-4B QA task (b) Mistral-7B Dialogue task (c) Mistral-7B QA task

Figure 5: Val set. Accuracy vs Prototype Size Z'

ence, a k-NN retriever pulls the most similar annotated examples as ICL demonstrations for each test query. **TopK+ConE** Peng et al. (2024) first retrieves the M most semantically similar candidates to a test query via SBERT cosine similarity (TopK), then reranks them by computing the conditional entropy of the test input under the LLM itself selecting whichever demonstrations minimise the model's uncertainty about the test input, making the choice both data- and model-dependent.

C.2 Loss Ablations

We isolate the contribution of each component of GA-ICL by evaluating four configurations (Table 6), all trained for the same 200-epoch budget where applicable: (1) Clustering, a non-learned baseline that selects demonstrations closest to the raw class mean in the original embedding space, representing prototype-based selection with no learned geometry at all; (2) proxy-anchor loss only, which learns class prototypes but with no manifold-preserving objective; (3) proxy-anchor loss + manifold point-to-point loss, without prototype dimensionality reduction (full latent dimension); and (4) the complete GA-ICL method, adding dimensionality reduction on top of both losses. Results across Qwen3-4B (HaluEval QA) and Mistral-7B (HaluEval Dialogue, QA) are shown in Table 6. Several findings emerge. First, moving from unlearned class-mean selection (Clustering) to a learned proxy-anchor geometry already yields a substantial improvement (e.g., +14.7 points on Qwen3-4B QA), showing that learned prototype-based selection alone provides most of the benefit over naive prototype selection. Second, adding the manifold-preserving loss provides a further, consistent gain (+2.1 to +2.7 points) on top of proxy-anchor learning, confirming that modeling local

Table 6: **Loss ablations** Ablation study showing the contribution of each component in the proposed GA-ICL framework.

Model	Task	Clustering (class-mean)	Proxy-Anchor Loss only	+ Manifold Loss	Full GA-ICL (dim. reduction)
Qwen3-4B	QA	50.5	65.2	67.3	71.2
Mistral-7B	Dialogue	50.4	52.3	55.0	68.8
Mistral-7B	QA	51.3	50.7	53.2	62.3

manifold structure contributes independently of prototype learning. Third, prototype dimensionality reduction contributes the largest share of the remaining gain (+3.9 to +13.8 points), consistent with our dimensionality analysis in Section 3.2 (Figures 5b- 5a). Together, these results show that GA-ICL's performance arises from the combination of all three components rather than any single one, with learned prototype geometry, manifold preservation, and dimensionality-aware compression each contributing distinct, additive value. All configurations were trained under the same epoch budget (200 epochs) to ensure a fair comparison. We note that the momentum proxy θ_m is used only for stable prototype updates during training via momentum averaging and is not itself a separate ablatable component; the retrieval-relevant geometry is defined by θ_q and the projection network h_θ.

C.3 Initialization comparison

Class prototypes θ_q are randomly initialized. We also evaluated class-centroid (mean-based) initialization as an alternative across both Qwen3-4B and Llama3-8B on all three HaluEval tasks. As shown in Table 7, reporting accuracy averaged over the same 5 random seeds used elsewhere in our analysis, centroid initialization consistently requires 15–30% more training epochs (230–260 vs. 200, tightly consistent across seeds within ±1–2 epochs) to converge, while yielding final accuracy within 0.2–0.6 points of random initialization across every setting. We therefore adopt random initialization as the default, since it reaches equivalent solution quality with less training overhead. The observed standard deviation for GA-ICL is approximately 1–2 accuracy points across models and tasks, larger than the 0.2–0.6 point gap between initialization strategies in Table 7. Taken together, these results indicate that GA-ICL's learned retrieval geometry is not meaningfully sensitive to prototype initialization, whether varying the initialization strategy itself or the random seed used within it: the strategy-level difference falls within the method's natural run-to-run variance.

Table 7: **Initialization comparison** - Comparison of Random Initialization and Mean/Centroid Initialization across models and tasks.

Model	Task	Random Init	Mean/Centroid Init		
(Epochs, Acc)					
(Epochs, Acc)		Δ Epochs	Δ Acc		
Qwen3-4B	Dialogue	200, 72.3	250, 71.8	+25%	-0.5
Qwen3-4B	Summ.	200, 57.7	260, 57.5	+30%	-0.2
Qwen3-4B	QA	200, 71.2	250, 70.9	+25%	-0.3
Llama3-8B	Dialogue	200, 51.6	230, 51.4	+15%	-0.2
Llama3-8B	Summ.	200, 52.3	240, 51.7	+20%	-0.6
Llama3-8B	QA	200, 68.7	240, 68.2	+15%	-0.5

C.4 Retreival baselines on Large models

We present the BM25 and KNN results for Phi-14B and Qwen3-32B, extending the Table 3 results in Section 3.2: With BM25 and KNN included, GA-ICL outperforms all baselines including lexical retrieval across both larger models on every task, including QA. This strengthens our claim in Section 4 that GA-ICL's QA limitation observed at smaller scale (Table 3) diminishes at larger model scale, since even BM25, which was competitive or superior to GA-ICL on QA at smaller scales, no longer closes the gap on Phi-14B or Qwen3-32B.

Table 8: **Extended evaluations** - Comparison of retrieval strategies across different models and tasks (accuracy in %)(averaged across 5 random seeds).

Model	Task	BM25	KNN	GA-ICL (Ours)
Phi-14B	Dialogue	71.4 ± 0.2	67.6 ± 0.3	$\mathbf{75.6 \pm 0.4}$
Phi-14B	Summ.	60.9 ± 0.2	61.3 ± 0.2	$\mathbf{65.6 \pm 0.3}$
Phi-14B	QA	72.4 ± 0.1	69.3 ± 0.3	$\mathbf{81.3 \pm 0.3}$
Qwen3-32B	Dialogue	78.3 ± 0.2	72.6 ± 0.1	$\mathbf{83.6 \pm 0.2}$
Qwen3-32B	Summ.	61.6 ± 0.1	61.2 ± 0.2	$\mathbf{67.4 \pm 0.3}$
Qwen3-32B	QA	67.4 ± 0.24	64.6 ± 0.2	$\mathbf{71.8 \pm 0.2}$

C.5 Random baselines

We additionally ran an empirical random baseline (2-shot, one demonstration sampled uniformly at random per class, 5 seeds) to capture realistic prompt-level variance: We note the random baseline's

Table 9: **Random baseline** - Performance (%, mean $\pm$ standard deviation) across different tasks.

Model	Dialogue	Summarization	QA	FEVER
Qwen3-4B	53.7 ± 7.8	51.2 ± 5.9	57.1 ± 6.3	60.2 ± 3.9
Llama3-8B	48.7 ± 4.6	49.3 ± 5.4	55.8 ± 6.5	59.3 ± 3.5

variance (σ = 3.5–7.8) is 2–6× higher than GA-ICL's ($\sigma \approx$ 1–2, Table 3), underscoring that GA-ICL's global prototype selection provides not only higher mean accuracy but substantially more stable demonstration selection across runs.

C.6 Random projection control

For the 3 configs mentioned in Figure 5a- 5b- 5c , we ran the random projection control: (Table 10) replacing the learned projection network h_θ with a fixed random linear projection (untrained weights, randomly-initialized prototypes) at each of the same target dimensions used in Figure 5a– 5c.

Random projection performs substantially and consistently worse than GA-ICL at every matched dimension by 9–16 points on Qwen3-4B QA and, on Mistral-7B QA, by up to 7 points at most dimensions (one dimension shows a small -2.2 point inversion, which we report for full transparency) and shows no coherent trend as dimensionality decreases, fluctuating within a noisy band rather than improving, in contrast to GA-ICL's consistent monotonic improvement as Z' shrinks. These results suggest that the improvements are not explained by generic dimensionality reduction alone, since a fixed random projection at the same target dimensions fails to reproduce the observed gains. Instead, the learned projection consistently produces higher performance, indicating that the geometry learned by GA-ICL captures task-relevant structure beyond simple compression. While this does not conclusively establish the underlying cause of the lower-dimensional effect, it provides empirical evidence that the improvements arise from the learned geometry rather than dimensionality reduction alone.

D Implementation details

The network h_θ, which is crucial in our method to sample the ICL demonstrations, is trained for 200 epochs on the training dataset D_{F_t}. Training utilizes two independent Adam optimizers: one for the network parameters and another for the proxy parameters. Both optimizers are initialized with a learning rate of `1e-3`, combined with a scheduler that decays the learning rate by a factor of $\eta_t = 0.97$. The dimensionality of the encoded vector Z is determined by the underlying Large Language Model (M). A mini-batch size of 128 samples is maintained throughout training.

Table 10: **Random projection vs GA-ICL** - Comparison of Random Projection and learned GA-ICL representations across latent dimensionalities for QA.

Model	Dim ($\times 10^3$)	Random Projection	GA-ICL (Learned)	Gap
Qwen3-4B QA	2.5	55.3	67.2	+11.9
	2.3	56.7	67.5	+10.8
	2.1	57.2	68.1	+10.9
	1.9	54.8	68.7	+13.9
	1.7	55.7	69.5	+13.8
	1.5	54.6	70.9	+16.3
Mistral-7B QA	3.8	52.5	53.4	+0.9
	3.6	58.4	56.2	−2.2
	3.4	51.6	56.4	+4.8
	3.2	54.2	58.7	+4.5
	3.0	53.1	60.1	+7.0
	2.8	57.8	61.3	+3.5
	2.6	55.9	61.9	+6.0

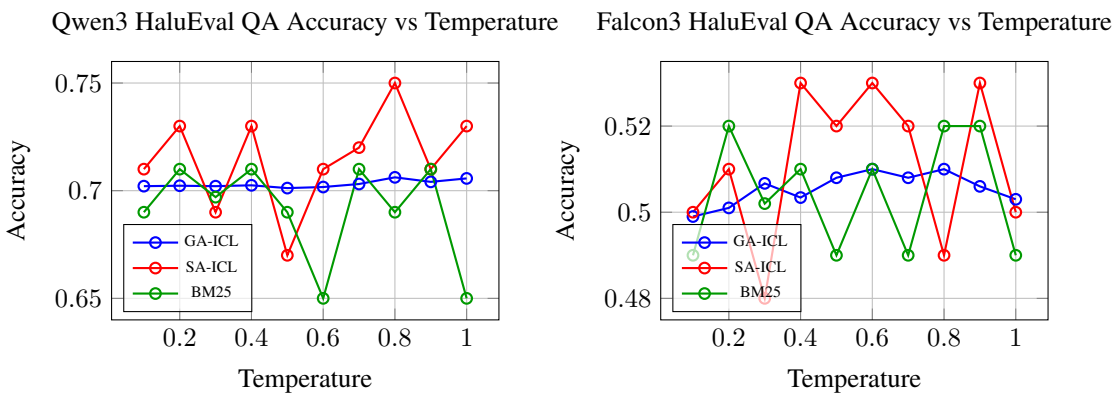

(a) Qwen3 HaluEval QA

(b) Falcon3 HaluEval QA

Figure 6: Accuracy vs Temperature comparison for Qwen3 and Falcon3 models on HaluEval QA dataset

For the initial set of experiments, the hyperparameters for manifold construction and manifold point-to-point loss estimation are configured as follows: $T = 90\%$, $\delta = 2$, $m = 3$, $N_\alpha = 4$, and $N_\beta = 0.5$. The momentum constant for updating θ_m is set to $\mu = 0.99$. For Proxy Anchor loss, we employ $\alpha = 32$ and $\epsilon = 0.1$. These settings serve as the baseline configuration.

All experiments were conducted on an NVIDIA RTX A6000 GPU. Training the lightweight neural network h_θ requires approximately 640 MB of GPU memory and about 3-4 hours of training time.

E Inference comparison of time taken and memory consumed

The Table 11 shows the inference time taken for each method on different tasks for Falcon-3-3B model.

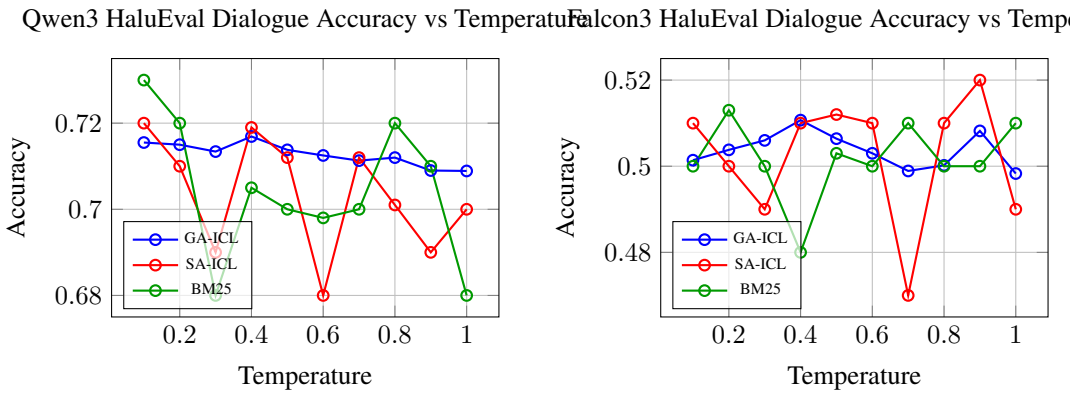

(a) Qwen3 HaluEval Dialogue task

(b) Falcon3 HaluEval Dialogue task

Figure 7: Accuracy vs Temperature comparisons for Qwen3 and Falcon3 models on HaluEval Dialogue dataset

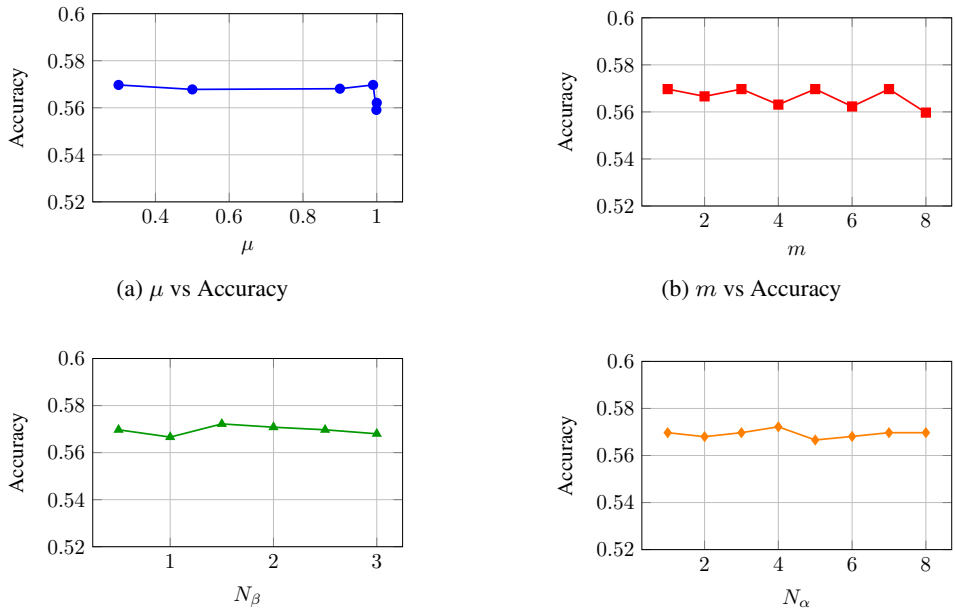

(a) μ vs Accuracy

(b) m vs Accuracy

(c) N_β vs Accuracy

(d) N_α vs Accuracy

Figure 8: Hyperparameter tuning for Qwen3-4B on Summarization task

Task	Method	Time	Mem (MB)
FEVER	BM25	50 min	6584
	KNN	1 hr 30 min	6584
	Perplexity	55 min	9392
	GA-ICL	**25 min**	**6574**
HaluEval Summ.	BM25	7 hr	8196
	KNN	3 hr	9260
	Perplexity	2.3 hr	31178
	SA-ICL	3 hr	13574
	GA-ICL	**1 hr**	**7900**
HaluEval QA	BM25	1 hr	6769
	KNN	1 hr 20 min	6714
	Perplexity	55 min	29116
	SA-ICL	1 hr	9528
	GA-ICL	**25 min**	**6685**
HaluEval Diag.	BM25	1 hr	6778
	KNN	1 hr 20 min	6752
	Perplexity	55 min	30051
	SA-ICL	1 hr	9643
	GA-ICL	**25 min**	**6694**

Table 11: Inference time and memory usage across tasks and methods (Falcon-3-3B).